

1 Functional connectome reorganization after pontine stroke is 2 associated with better motor outcomes

3

4

March 15, 2021

5 Emily Olafson, Keith Jamison, Hesheng Liu, Danhong Wang, Joel Bruss, Aaron Boes, Amy Kuceyeski

6 Introduction

7 Motor deficits are the most common and disruptive symptoms of ischemic stroke. Spontaneous re-
8 covery of motor function occurs for most patients [1], and is dependent on the ability of brain networks
9 to functionally reorganize and compensate for lost function [2]. As demonstrated by animal models, the
10 functionality of damaged motor regions may be adopted by surviving tissue around the lesion, but brain
11 areas distant to the lesion with similar function and connectivity as the damaged area have also been shown
12 to compensate in animals, typically when the initial infarct is large [3, 4, 5, 6].

In humans, functional reorganization underlying post-stroke motor recovery has been studied with resting-state functional magnetic resonance imaging (fMRI). Strong evidence suggests that crucial to eventual motor recovery is the restoration of interhemispheric resting-state functional connectivity (FC) between the primary motor cortices [7, 8, 9], but less is known about how functional networks change on a greater spatial and temporal scale after stroke. Altered network topology [10] and recruitment of other networks aside from the motor network such as the frontoparietal network [11, 12] have been implicated in the recovery process, but network changes at a high temporal resolution have not been well documented.

Prior studies investigating neural correlates of motor recovery have focused almost exclusively on supratentorial strokes that impact the internal capsule and surrounding areas. Infratentorial pontine strokes, which impact the connections between motor cortex and the cerebellum [13], and account for roughly 7 percent of all ischemic strokes [14], may have different sources of motor deficits and mechanisms of recovery-related reorganization from those of supratentorial strokes. Reduced blood flow measured by arterial spin labeling has been observed in the cerebellum and cortical regions in pontine stroke [15, 16] and longitudinally, changes in cerebral blood flow in cortical areas including the supramarginal gyrus and middle occipital gyrus were related to motor recovery. Areas with abnormal blood flow over time also had abnormal FC [15], and increased degree centrality in the ipsilesional cerebellum has been related to better motor recovery [17]. The network changes associated with functional damage and subsequent recovery in pontine stroke have yet to be assessed in a longitudinal study.

Another key element of stroke recovery is diaschisis, a process by which remote brain areas anatomically connected to the lesion undergo structural and functional changes [18]. Functional impairment and subsequent reorganization of areas anatomically connected to the lesion may be an important component of the recovery process that is still being explored. In this study, we propose a novel measure to capture

38 adaptive functional plasticity after pontine stroke, outlined below, and connect it to patterns of structural
39 disruption after stroke.

40
41 Connectivity to the rest of the brain is one aspect of a brain region’s functional role in the network.
42 We propose that instances of functional reorganization over time, as in the case of adjacent surviving tissue
43 adopting the functional role of lost tissue, may be captured by identifying brain regions whose pattern of
44 FC with the rest of the brain is more closely matched by a different brain region at a later date. Considering
45 functional connectomes as graph, the task of identifying similar nodes (gray matter regions, in this case)
46 between two functional connectomes can be considered a graph matching problem [19]. Graph matching
47 has been applied recently to map individual structural connectomes to their functional connectomes [20].
48 Conceptually, the process of graph matching exchanges the labels of nodes when doing so results increased
49 similarity of the two networks. When two regions exchange FC profiles, the regions are said to have been
50 ‘remapped’. We hypothesize that brain regions with more structural damage due to the lesion will more
51 frequently functionally reorganize; that more impaired subjects will have more global functional reorganiza-
52 tion; and that the amount of functional reorganization will correlate with the change in motor impairment
53 between subsequent sessions.

54 Methods

55 Data description

56 Twenty-three first-episode stroke patients (34-74 years old; mean age 57 years; 8 female) with isolate
57 pontine infarcts. 15 subjects had right brainstem infarcts, 9 had left brainstem infarcts (Figure 1), and
58 is described previously [13]. Patients were scanned five times during a period of 6 months - 7, 14, 30, 90
59 and 180 days after stroke onset (Figure 2) on a 3T TimTrio Siemens using a 12-channel phase-array head
60 coil. Structural images were acquired using a sagittal MP-RAGE three-dimensional T1-weighted sequence
61 (TR, 1600ms; TE 2.15ms; flip angle, 9°, 1.0 mm isotropic voxels (FOV, 256 x 256). Each MRI session
62 involved two to four runs (360s each run) of resting-state fMRI. Subjects were instructed to stay awake and
63 keep their eyes open; no other task instruction was provided. Images were acquired using the gradient-echo
echo-planar pulse sequence (TR, 3000ms; TE, 30ms; flip angle, 90°, 3 mm isotropic voxels).

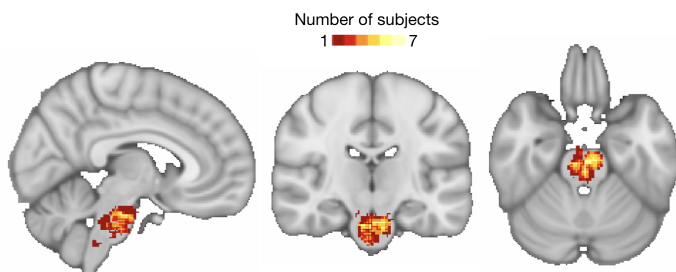


Figure 1: Distribution of lesions across the brain. Colors indicate the number of subjects with a lesion in that location.

64

65 Structural data processing

66 Preprocessing of the longitudinal structural data included registration of each subject’s session 2-5 T1
67 scans to the space of session 1, collapsing co-registered files to an average, creation of a skull-stripped brain
68 mask, followed by manual editing and binarization of the hand-edited mask. Each mask was then pushed to

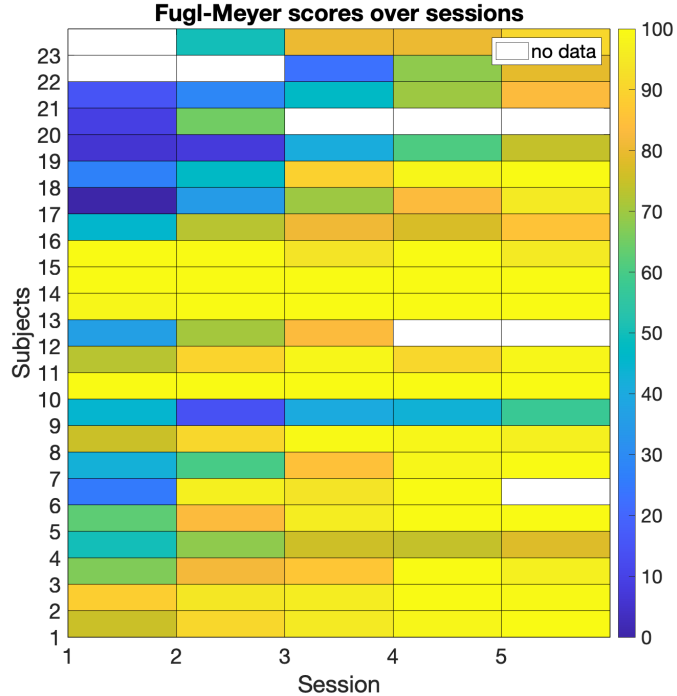


Figure 2: Fugl-Meyer scores for all subjects over sessions. Note that for subjects 6, 12, 20, 22, and 23 scores are missing. For subjects 6, 12, and 20, functional data is also missing

69 each of the session 2-5 T1s in native space using the inverse registration acquired from the first step. This
70 was followed by bias field correction of the 5 T1 scans, transformation of native-space bias field-corrected
71 data back to session 1 space, and the creation of an average bias field-corrected scan for each subject. Lesion
72 masks were hand-drawn on these transformed T1 scans by ADB and JEB.

73 Functional data processing

74 Preprocessing of the longitudinal functional data was performed using the CONN toolbox, including
75 functional realignment of volumes to the first volume, slice timing correction, segmentation and normalization,
76 smoothing with a 4mm FWHM kernel, followed by a denoising protocol (CompCor [**Behzadi2007-zt**])
77 which regressed out the CSF and WM signal, as well as realignment parameters. Temporal band pass filtering
78 (0.008 - 0.09Hz), motion correction, despiking and global signal removal regression were also performed.
79 Regional time series data was acquired by parcellating the scans into 268 non-overlapping brain regions
80 using a functional atlas defined for healthy controls [21] and averaging the time course of all voxels with a
81 region. Several analyses involve further parcellating of the 268-node atlas into 8 subnetworks [27] (Figure
82 S2).

83 Functional connectivity calculation

84 Functional connectivity (FC) matrices were calculated as the regularized inverse of precision matrices.
85 Calculating FC using precision minimizes the effect of indirect connections and has been shown to result in
86 FC that are more similar to structural connectivity [22, 23]. To compute the precision FC, we first took
87 the unregularized inverse of the correlation matrix for each subject and averaged them over the sample to
88 obtain the population-level precision matrix. We then calculated the individual's precision matrices using
89 Tikhonov regularization, which adds a positive term to the diagonal of the precision matrix before inversion

90 where I is the identity matrix and λ is the regularization parameter. Gamma $\gamma \in [0, 1]$ was chosen via a
91 grid search to be the value that minimized the root mean squared error of the Frobenius norms between
92 the regularized subject precision matrices and the population-level unregularized precision matrix, and was
93 found to be $\gamma = 0.58$ (Supplementary Fig S1).

94 **Estimated structural disconnection**

95 Deficits from subcortical stroke may be related to damage at distant sites via metabolic diaschisis
96 [24, 25]. In order to account for the impact of lesions on the structural connectome, the extent of regional
97 structural (white matter) connectivity disruption due to the lesion was assessed for each stroke subject with
98 the Network Modification (NeMo) Tool [26]. The Network Modification (NeMo) Tool v2 requires only an
99 individual's lesion mask in MNI space, which was obtained as described above, to produce an estimate
100 structural disconnection for each brain region. The newest version of the NeMo Tool, originally published
101 in 2013, includes a reference database of connectivity networks from 420 unrelated individuals from the
102 Human Connectome Project's (HCP) 1200 release (50 percent female, aged 25-35). The NeMo Tool begins
103 by mapping the lesion mask into this healthy database's collection of tractography streamlines that quantify
104 likely white matter pathways. It then identifies streamlines that pass through the lesion mask and records
105 the gray matter regions that are at end of that streamline. Thus, the NeMo Tool produces the regional
106 structural disconnection vector (ChaCo score, Change in Connectivity) that is an estimate of the percent
107 of damaged streamlines terminating at each region in the atlas.

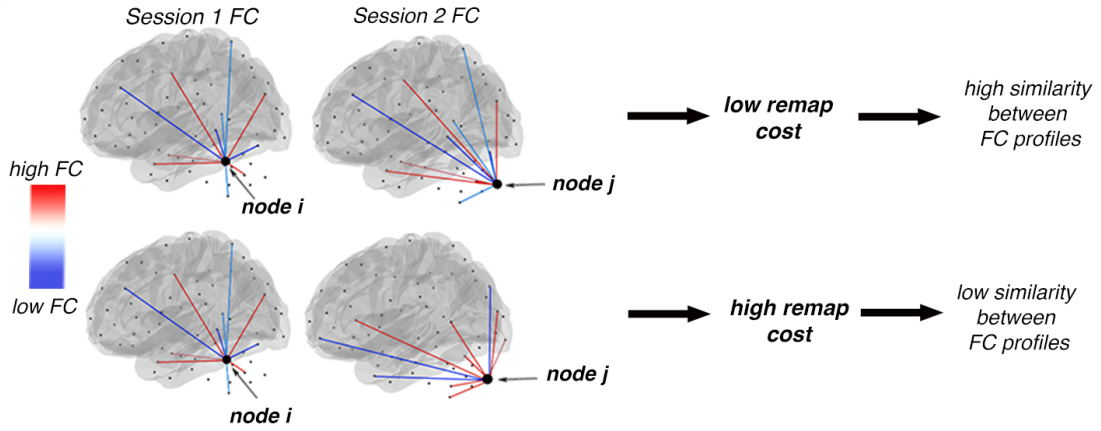
108 **Graph matching**

109 We propose the use of graph matching to capture FC network reorganization over time; graph match-
110 ing has recently been used in brain connectivity networks to map SC to FC [20]. Graph matching is an
111 algorithmic process that maximizes the similarity between two networks by identifying a mapping between
112 similar nodes in the two networks. One approach to identifying the optimal mapping that maximizes the
113 similarity between two networks is with a combinatorial optimization problem known as linear assignment.

114 Take two $n \times n$ networks A and B and a cost function $c : A \times B \rightarrow \mathbb{R}$ that determines the cost of
115 assigning each node in A to each node in B . Here, our cost function is the sum of the entries in the cost
116 matrix $C = (c_{ij})$, whose entries are defined by the Euclidean distance between all pairs of rows, representing
117 each node's FC profile, in A and B , i.e. $c_{ij} = \|A_{i\bullet} - B_{\bullet j}\|_2^2$. In this formulation, the linear assignment
118 problem aims to construct the permutation matrix $P = (p_{ij})$ that minimizes the sum of the elements in cost
119 matrix, i.e. $\min_P \sum_{i=1}^n \sum_{j=1}^n c_{ij} p_{ij}$. The matrix P is a permutation matrix with exactly one entry equal
120 to 1 in each row and column, and all the rest being zero. Ones in the diagonal mean the same node in the
121 two networks were mapped to one another, while ones in the off-diagonal indicate two different nodes were
122 "remapped" to one another.

123 Here, we will use the Hungarian algorithm to solve this minimization problem and find the cor-
124 responding optimal permutation matrix. Figure 3 illustrates how the graph matching will be applied to
125 subsequent longitudinal FC networks (from 1 week to 1 month and 1 month to 6 months) from each stroke
126 and control individual. In the top row of Figure 3 the two brain regions (black spheres, labeled node i and
127 node j) have very similar functional profiles, depicted with red and blue lines to other regions, and thus the
128 cost of remapping them is low. In the second row of 3, the two brain regions have very different functional
129 profiles and thus the cost of remapping them is high. An example cost matrix from a stroke subject's FC
130 extracted from 1 week MRI and FC extracted from 1 month MRI is provided in (Figure S6). Unsurprisingly,
131 the lowest costs are along the diagonal (the same region mapping to itself between time points) and across
132 left-right homologues (in the prominent super and sub diagonals).

A



B

Given two **sets of nodes A, B** and a **cost function c** that determines the cost of assigning each node in A to a corresponding node in B, graph matching finds a one-to-one mapping function $f : A \rightarrow B$ that minimizes the sum of all the matches between A and B

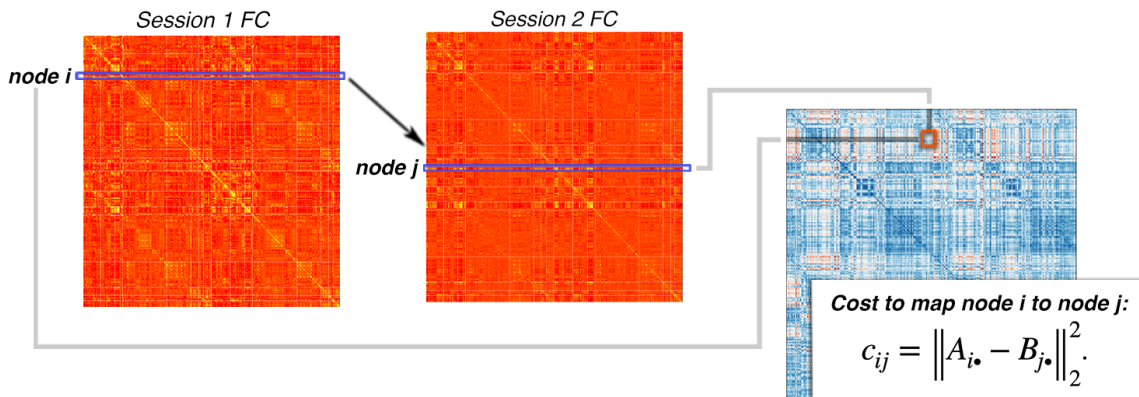


Figure 3: Graph matching procedure

133 **Estimation of functional reorganization**

134 The permutation matrices calculated for each pair of time points for each individual were used as a
135 measure of functional reorganization. To assess the spatial pattern of reorganization, the number of times
136 each node was remapped across all subjects was calculated as the 'remap frequency', where nodes with a
137 greater remap frequency are assigned to alternative nodes in the subsequent time point. For each subject
138 the number nodes that were remapped can be calculated as a subject-specific measure of the extent of
139 functional reorganization. Inspection of the patterns in the off-diagonal allows for identification of region
140 pairs that may be remapping over time (Figure S6).

141 **Code availability**

142 The code for partial functional connectivity calculation, graph matching, and remap frequency is
143 available on GitHub: <https://github.com/emilyolafson/stroke-graph-matching>

144 **Results**

145 **Brain areas with greater structural disruption reorganize more frequently**

146 Functional remapping frequency scores were highest in the brainstem and cerebellum, and to a lesser
 147 extent in the motor cortices (Figure 4a), similar to the spatial distribution of ChaCo (structural discon-
 148 nection) scores, which were also highest in the brainstem and cerebellum (Figure S3). For each pair of
 149 longitudinal, subsequent time points, there was a significant, positive correlation between average regional
 150 ChaCo scores across subject and functional remapping frequency, indicating those regions with more base-
 151 line structural connectivity disruption also had more remapping over time (Figure 4b). Furthermore, for
 152 about 50 percent of subjects, the nodes that remap have significantly higher ChaCo scores compared to
 153 those that do not remap (Figure S4).

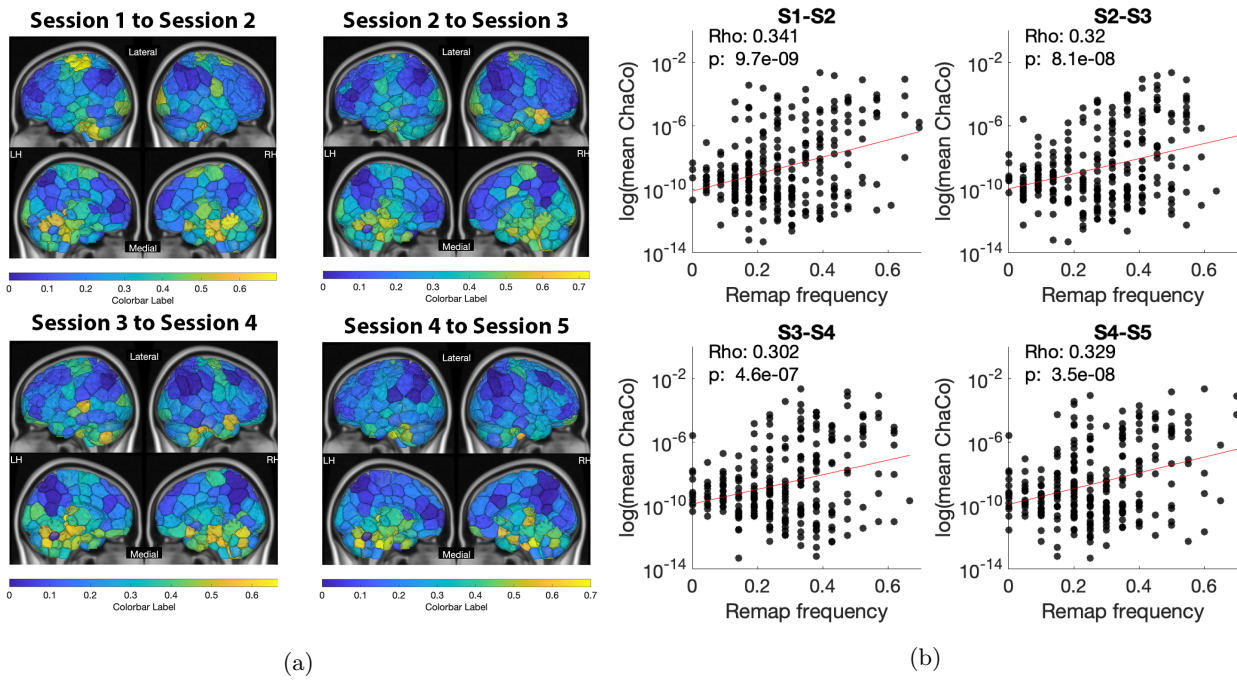
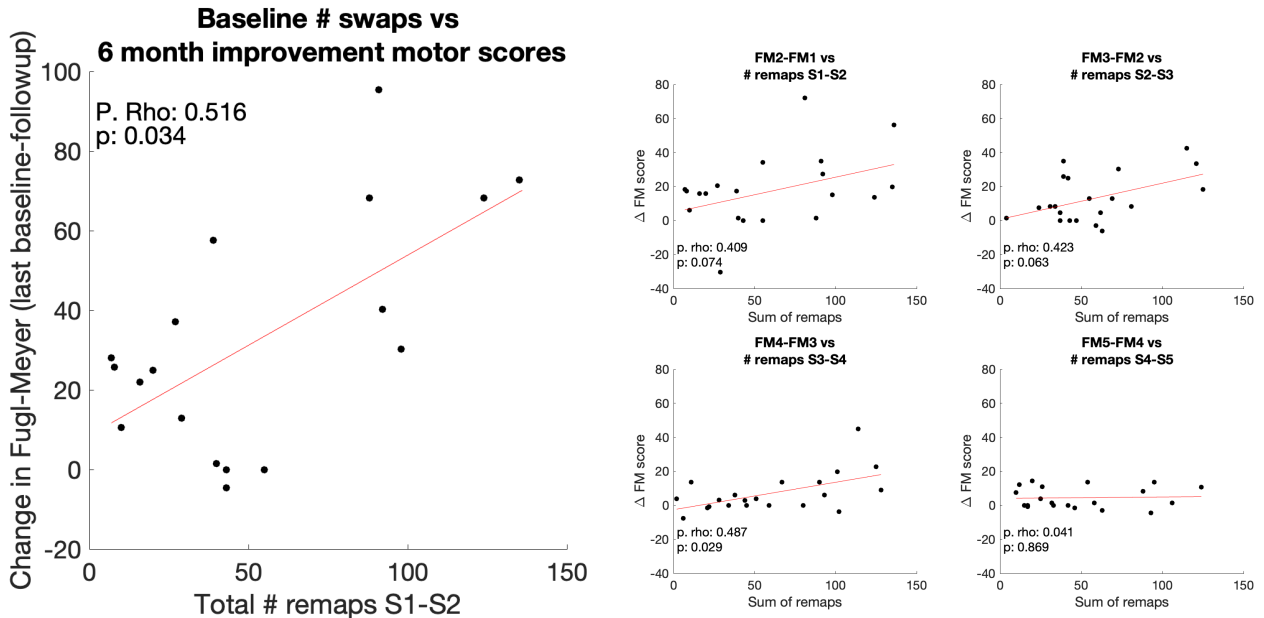


Figure 4: Remap frequencies are related to estimated structural disconnectivity. A) Node remap frequencies plotted on a glass brain for each session comparison. Inset figures display a lateral view (top row) and medial view (bottom row). B) Correlations between average ChaCo scores and node remap frequencies.

154 **Permutation matrices**

155 The most consistent pattern observed across subjects is that nodes are most frequently assigned
 156 to themselves (Figure S5). Nodes which do not map to themselves, which can be observed as non-zero
 157 indices in the off-diagonal of permutation matrices (Figure S5), more frequently occur between contralateral
 158 hemispheres than within the same hemisphere. We also assessed patterns of remapping within 8 functional
 159 networks by calculating the total number of swaps across subjects that involve nodes in the same network
 160 . The most remaps occur within and between nodes in the subcortical-cerebellum network, followed by the
 161 motor network, with the most remaps occurring between session 2-3 for both the subcortical-cerebellum and
 162 motor network (Figure S7).



(a) Partial correlation between the total number of remaps observed between session 1 and session 2 and the different in Fugl-Meyer scores between session 1 and session 2 ($FM_2 - FM_1$), controlling for subjects' average scan lengths between session 1 and session 2.

(b) Partial correlation between the total remaps observed between each pair of time points and the change in Fugl-Meyer scores between time points, controlling for scan length.

Figure 5: The amount of functional remapping between scans is related to impairment at baseline and to recovery between sessions.

163 Functional reorganization is related to impairment and recovery

We observed a significant positive correlation between baseline impairment, as measured by the Fugl-Meyer assessment at 7 days post stroke, and the number of remaps, such that patients who were more impaired at 7 days post-stroke had more remapping over the second week post-stroke (Figure 5a). The amount of recovery between subsequent sessions was positively associated with the number of remaps between sessions (Figure 5b). There was a modest correlation between the mean scan length between sessions (after motion scrubbing) and the number of remaps observed, such that longer scans had fewer remaps. Because all subjects had varying numbers of scans and therefore scan lengths, we performed these analyses using partial correlations, controlling for mean scan length between imaging sessions.

172 Remapping in control subjects

We performed the same graph matching analysis in 3 separate datasets of healthy control individuals: the first of a single female individual sampled for 30 continuous days, then in three separate individuals sampled between 10 and 14 days (from Newbold et al., 2020) and in 8 individuals sampled over 10 days (NSD).

Because of the repeated scans, 6 non-overlapping windows of both 7 days (replicating session 1 - session 2) and 14 days (replicating session 2 - session 3) were extracted (Supplementary methods).

179 Penalizing swaps based on distance does not substantially alter results

Prior animal work suggests that functional remapping more often occurs in areas proximal to the lesion site. As such, we added a bias to the graph matching procedure that increased the cost of mapping

182 to nodes proportional to their distance (Supplementary methods). Several β parameters were chosen based
183 on their impact on the amount of remapping observed (Figure S10). Increasing β reduced the total number
184 remaps, particularly the number of contralateral remaps (Figure S11) and had a similar effect across time
185 points. The main results replicated across increasing distance bias (Figure S12, S13, S14).

186 Sources of noise

187 The impact of noise from lesions impacting the BOLD signal of underlying gray matter is likely not
188 driving remapping, as the maximum overlap of the lesions with each ROI is no more than 30 percent (not
189 shown) and the average percent lesion overlap with each ROI across subjects does not correlate with remap
190 frequency (Supplementary fig). Lesion size is also unrelated to the number of remaps for each subject
191 (Figure S8a), but the lesion load on the corticospinal tract does positively correlate with the amount of
192 reorganization between session 1 and 2 (Figure S8b). We also found that the number of remaps was not
193 related to motion as measured by framewise displacement (Fig S9).

194 Discussion

195 Limitations

196 There are several limitations to this study. The first is that the impact of noise cannot be completely
197 accounted for due to a lack of sufficient controls with the same acquisition and processing methods. It is
198 possible that the nodes that remap more frequently are in brain areas that have lower SNR and that remaps
199 observed as indicative of noisy signal. Indeed, the SNR of HCP subjects is lowest in medial structures such
200 as the thalamus, cortical midsurface, and most consequentially to this study, the anterior cerebellum (see
201 S15). However, the motor network has relatively higher SNR in the HCP analyses and was contained a
202 substantial proportion of the total remaps across subjects (second to the subcortical/cerebellum network)
203 suggesting that remaps may be true signal.

204 Supplementary Methods

205 Regularization based on distance

206 We replicated the analyses of the main paper after adding a regularization parameter to each node
207 pair based on the Euclidean distance between the mean coordinates of the region in MNI space. Specifically,
208 the Euclidean distance between two nodes i and j , in physical space, E_{ij} multiplied by a constant β was
209 added to the cost matrix c_{ij} such that the new cost matrix equation was $c_{ij} = \|A_{i\bullet} - B_{\bullet j}\|_2^2 + \beta E_{ij}$. As such,
210 the cost of remapping nodes that are farther apart is higher. The analysis was repeated with β parameters
211 of 0, 1e-4, 2e-4, and 3e-4 with corresponded roughly to remap proportions of roughly 0.3, 0.10, 0.08, and
212 0.05, respectively.

213 28andMe control analysis

214 28andMe data [] was used due to insufficient control data. This dataset consists of a densely sampled
215 female participant (23 y.o.) who underwent imaging for 30 consecutive days. Raw data was unavailable,
216 but parcellated timeseries were obtained. fMRI preprocessing is detailed in [Pritshcet] and details do not
217 deviate significantly from the processing described in this paper (same softwares used). GSR was performed
218 on the timeseries data. Because the TR for the resting state fMRI obtained for this subject was much lower
219 than the TR of stroke subjects (720ms vs 3000ms, respectively), the 28andMe data was downsampled to
220 an equivalent TR. Initial scans contained 820 frames at a TR of 720ms, roughly 10 minutes of acquisition.

221 Downsampling to keep 1 out of every 4 TRs (equivalent TR of 2880s) reduced the number of frames to
222 205, bringing it into the range of the stroke subjects (173-300 TRs). A stable regularized precision matrix
223 calculation could not be performed, so the 28andMe analyses were completed using functional connectivity
224 derived from the linear correlation between node time series.

225 **Cast data**

226 subject 1 - subject 2 - 12 pre-cast days. - 1 and 8, 2 and 9, 3 and 10, 4 and 11, 5 and 12 for S1-S2
227 - day 27 to day 63 = post-cast 27 to 41, 28 to 42, 29 to 43... etc S2-S3 Raw data was downloaded from
228 datalad and processed with the same pipeline as the stroke subjects. MSC participants were scanned using
229 a 3T Siemens Trio MRI scanner. BOLD data were acquired at a spatial resolution of 4mm, single-band,
230 with a TR of 2.2s. We used identical sequences for sub-cast1 during the original cast experiment (but
231 not during the later control experiment). a new MRI scanner became available. sub-cast2 and sub-cast3
232 were scanned on a 3T Siemens Prisma using new sequences. The updated scanner and sequences were also
233 appleid to sub-cast1 during the later control experiment. BOLD data for these scans were acquired at a
234 spatial resolution 2.4mm, multi-band 4, with a TR of 1.1s.

²³⁵ **Supplementary Figures**

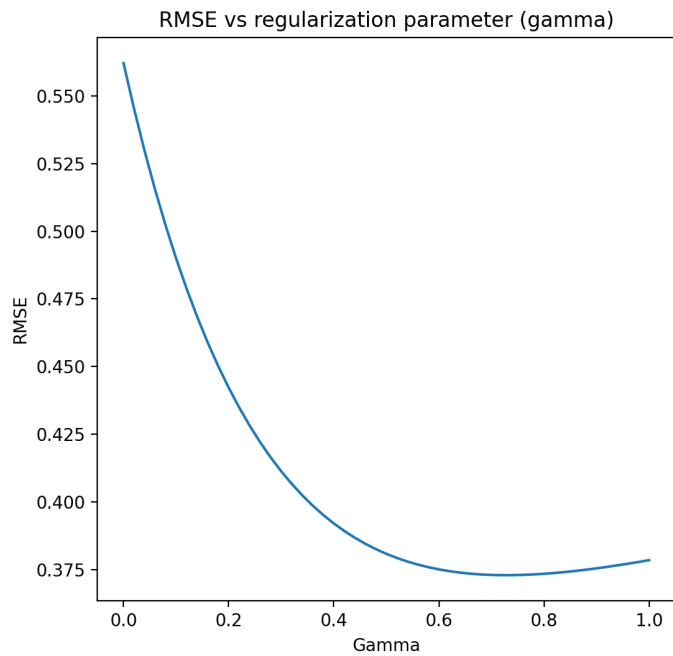


Figure S1: Results of gridsearch for gamma; plotted is the root mean squared error (RMSE) across subjects of the norm of each subject's precision matrix and the group average unregularized precision matrix at each lambda. The optimal gamma that minimized the RMSE across subjects was 0.58

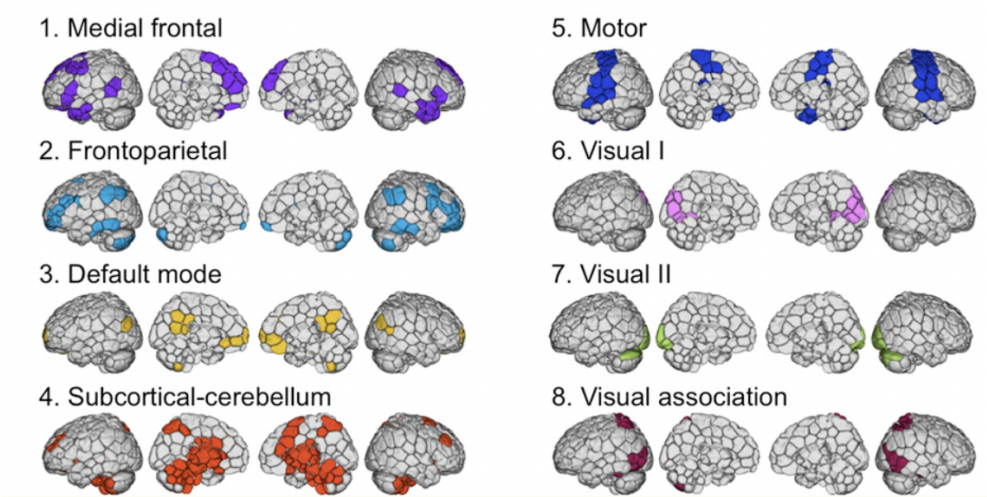


Figure S2: 8 functional networks identified by [27] by clustering healthy functional connectivity matrices.

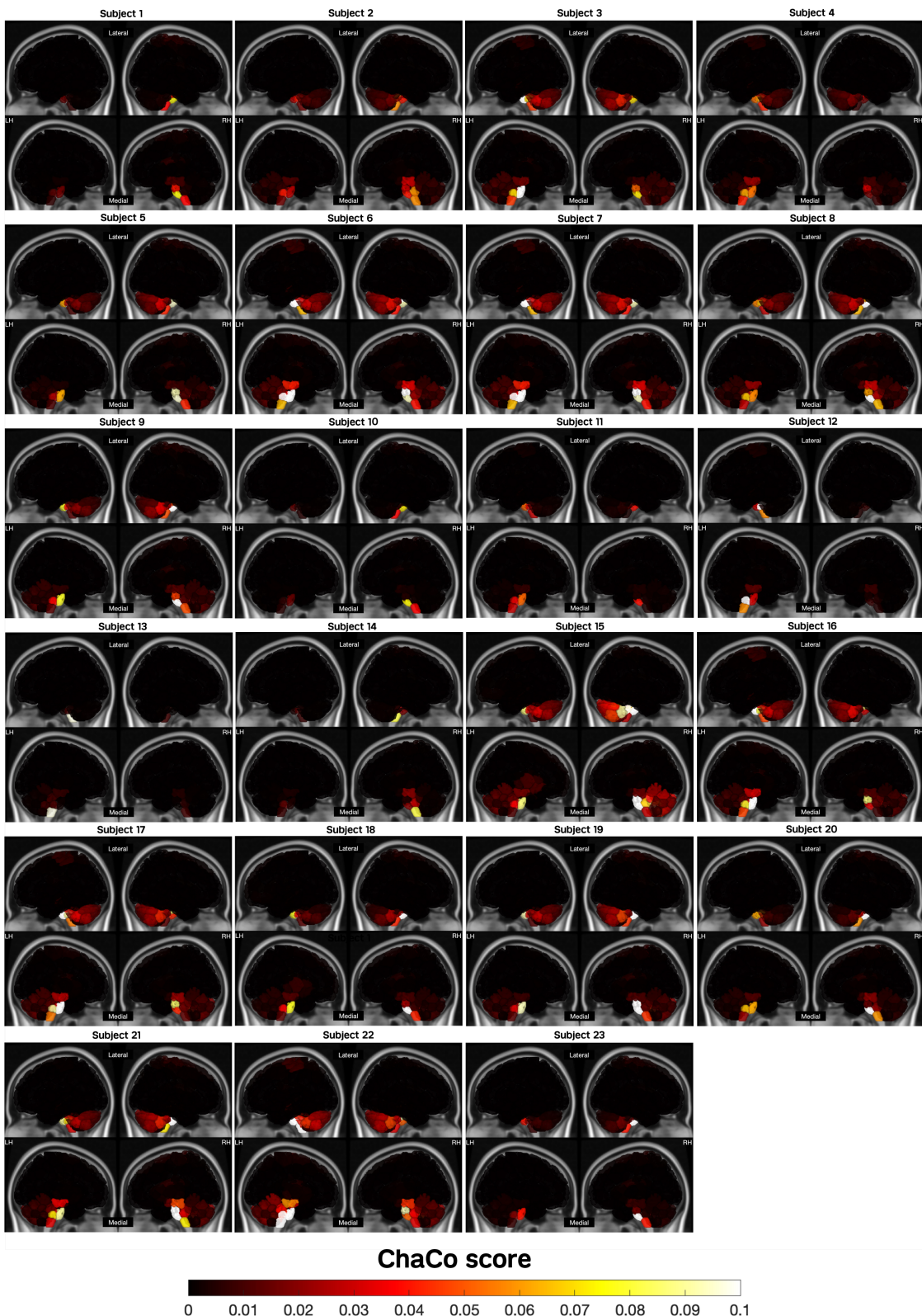


Figure S3: Regional ChaCo scores of all subjects displayed on glass brains displaying the number of streamlines terminating in each region that intersect with the lesion, normalized for the total number of streamlines terminating in that region. Top row of each subject inset: lateral view, bottom row of each inset: medial view.

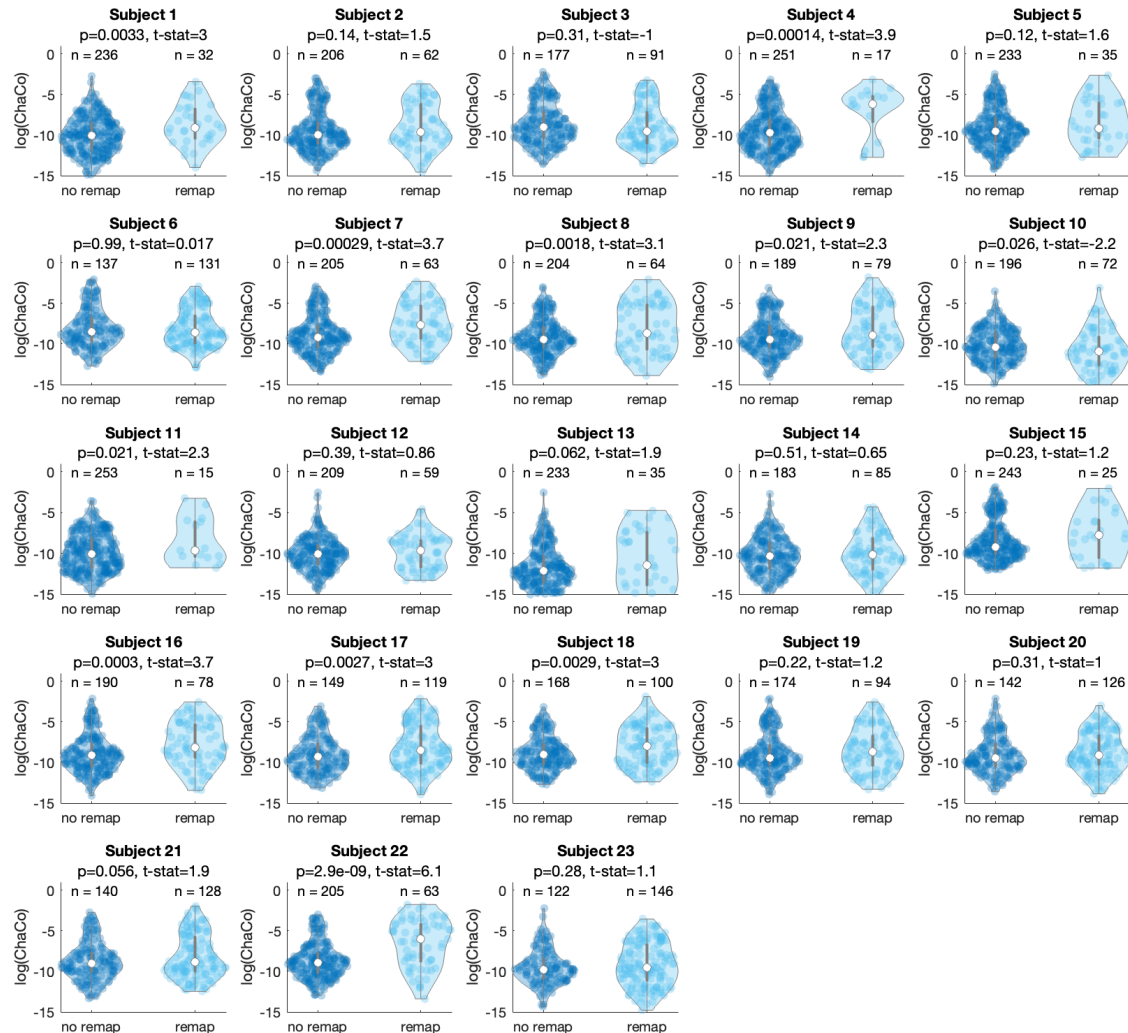


Figure S4: Paired t-tests determining whether there is a significant difference between the ChaCo scores of nodes that remap to different nodes versus those that do not. Remap patterns for the comparison between session 1 and 2 are shown; similar results are observed for other time points. No FDR correction

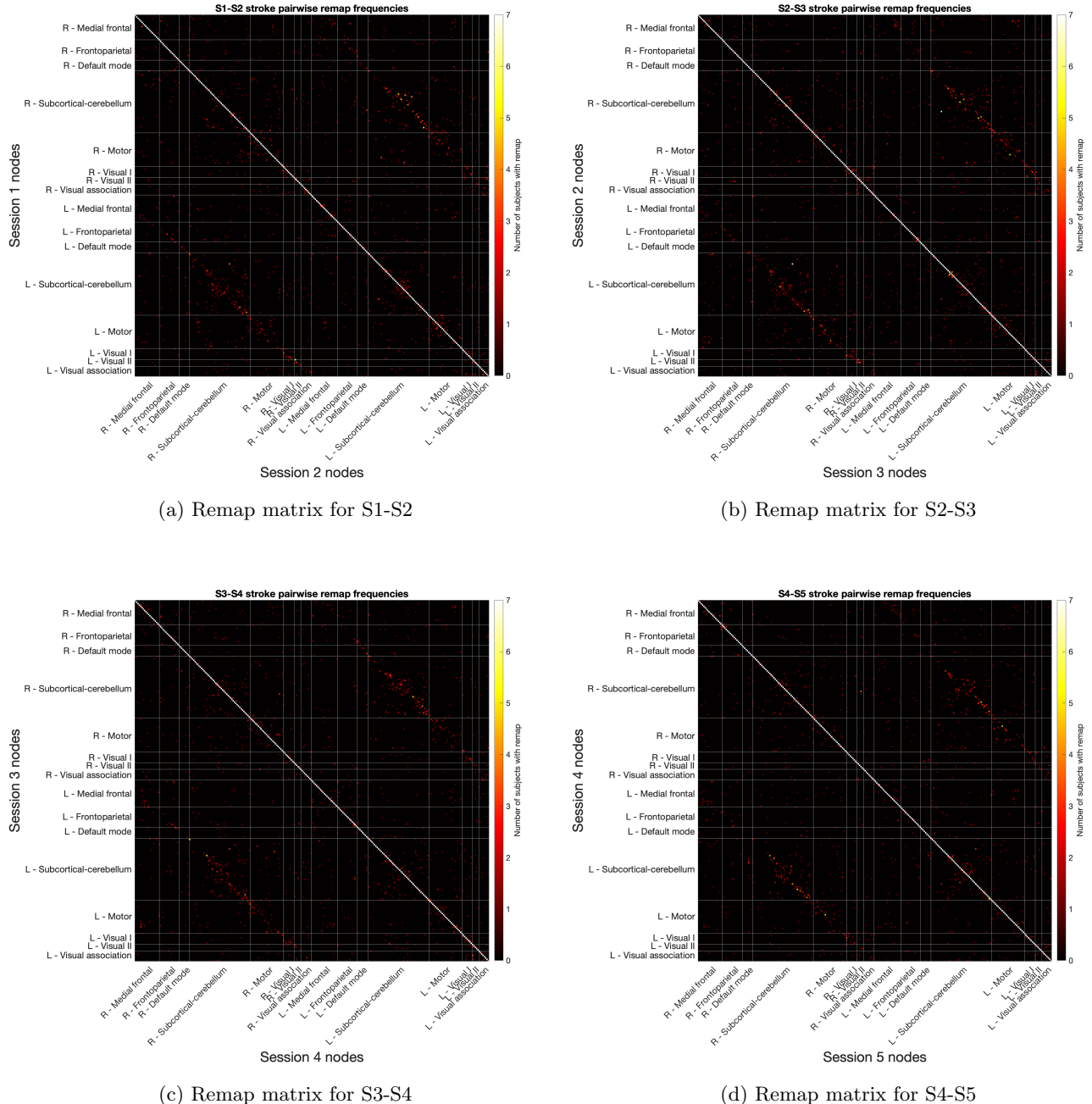


Figure S5: Permutation matrices across all 23 subjects. Each row and column represents the number of subjects where that specific remapping (node i = row i to node j = column j). The colorbar was cutoff at 7 subjects to improve visibility of off-diagonal elements.

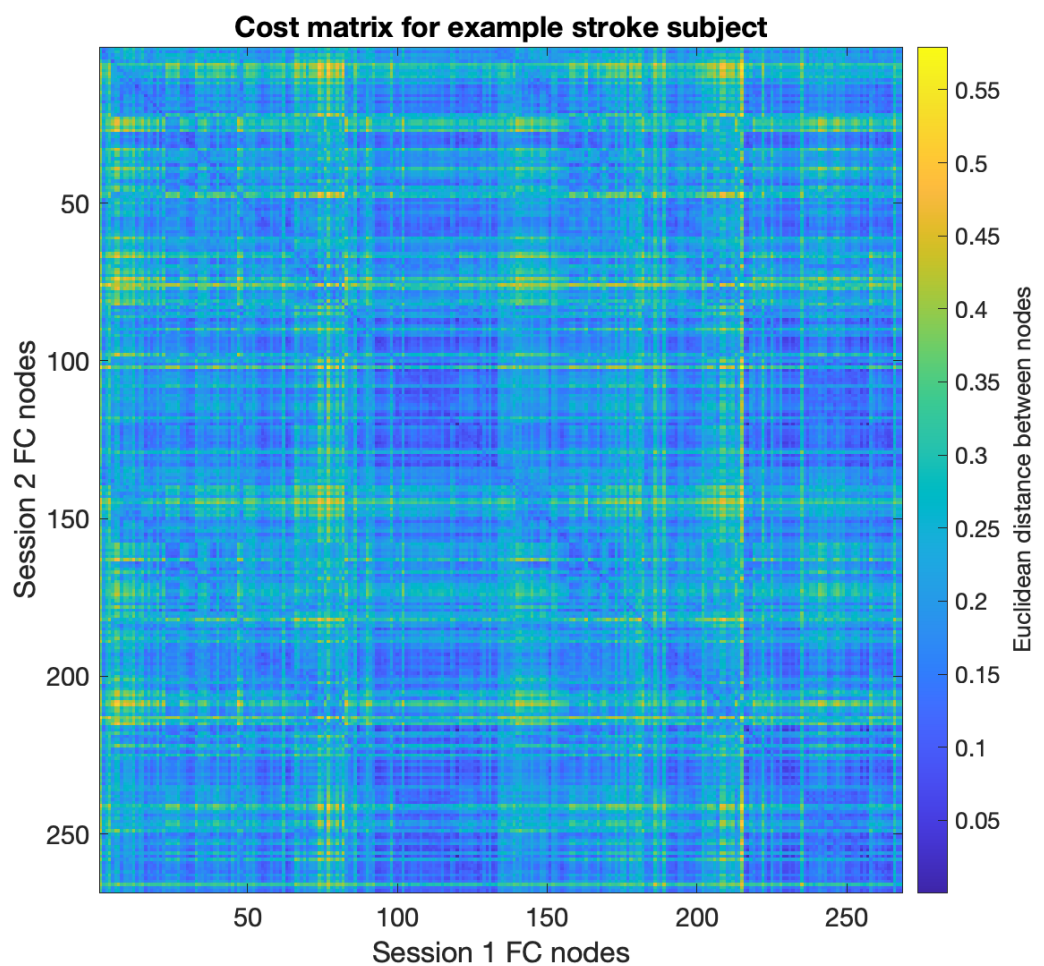


Figure S6: Cost matrix indicating the cost of remapping nodes from session 2 (vertical axis) to every other node in session 1 (horizontal axis).

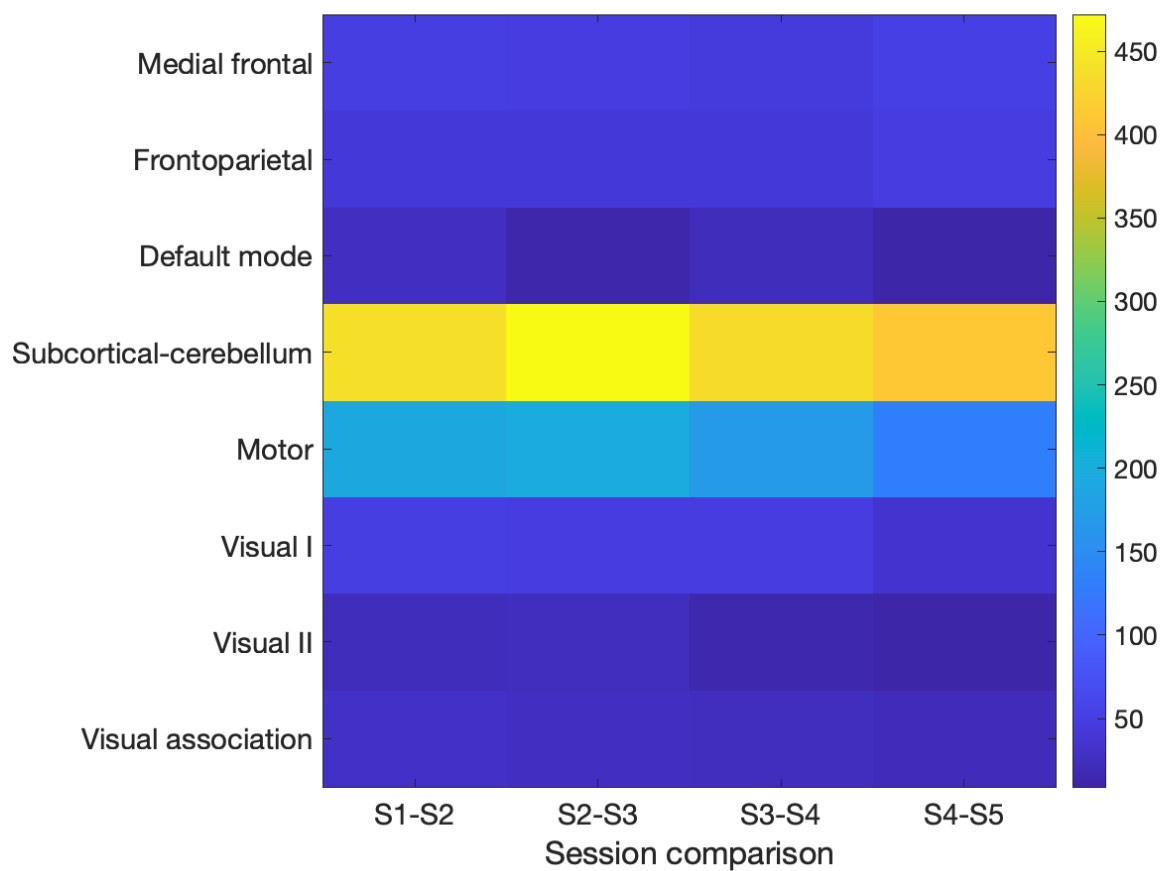
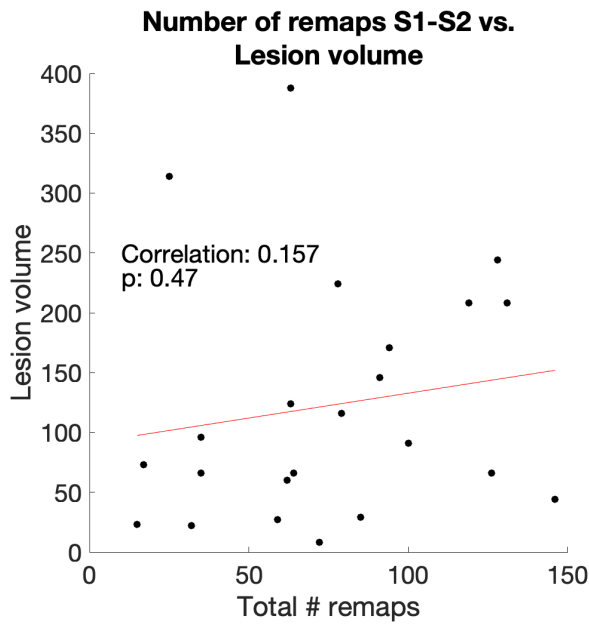
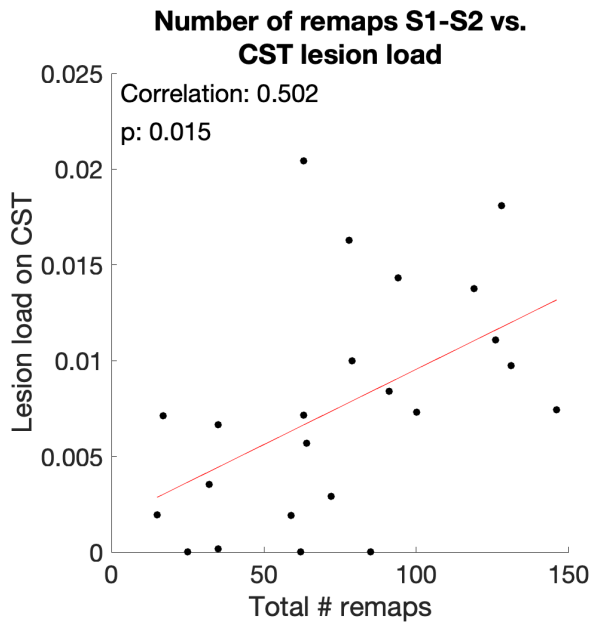


Figure S7: Sum of remaps within 8 functional networks; values in cells represent the total number of swaps between nodes in each network (only including off-diagonal remappings that occur within the same network; i.e. original and target nodes are in the same network) across subjects.



(a) Lesion volume in mm³



(b) Lesion load on the CST calculated as the proportion of the CST that intersects with the binary lesion mask (calculated on the ipsilesional CST)

Figure S8: The extent of the lesion's impact on the ipsilesional corticospinal tract is associated with the number of remaps between session 1 and 2 whereas the total lesion volume is not.

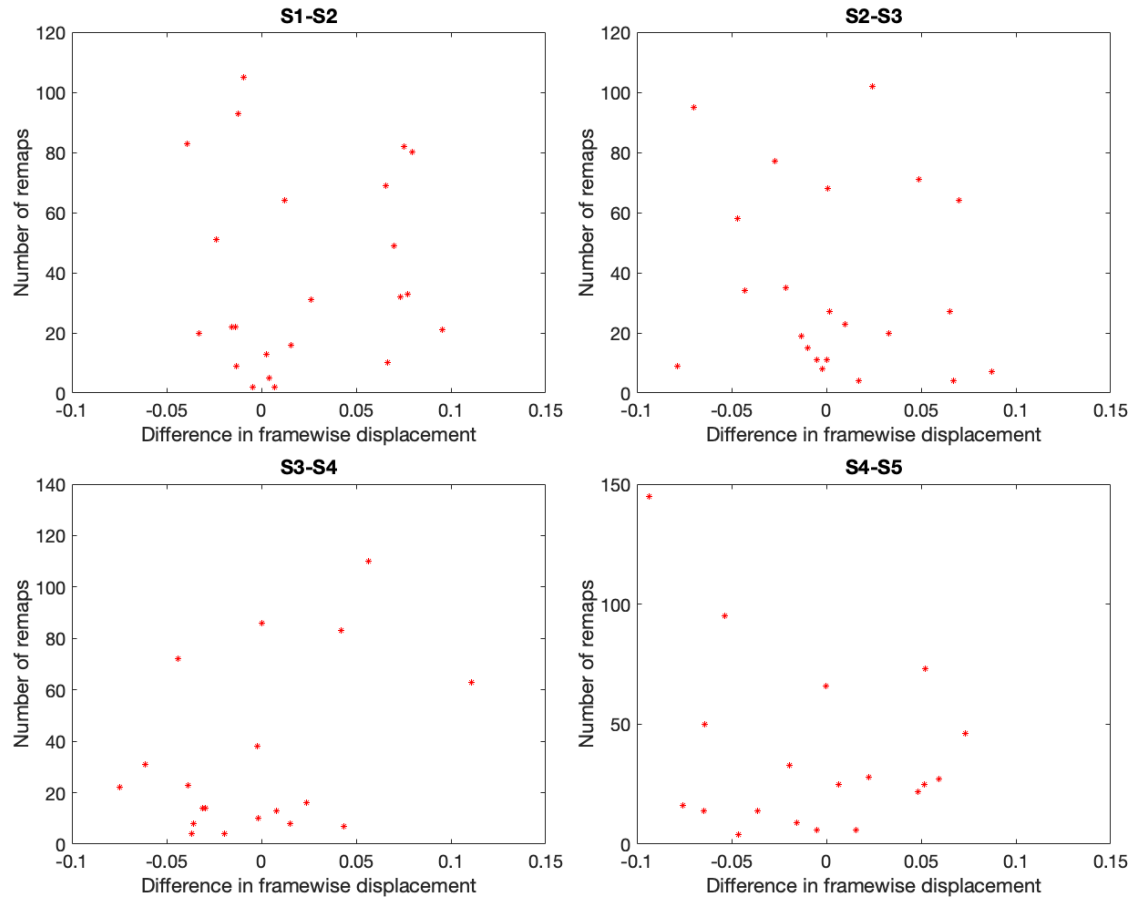


Figure S9: Correlation between difference in motion (as measured by framewise displacement) between 2 scans and the amount of remaps between the two scans.

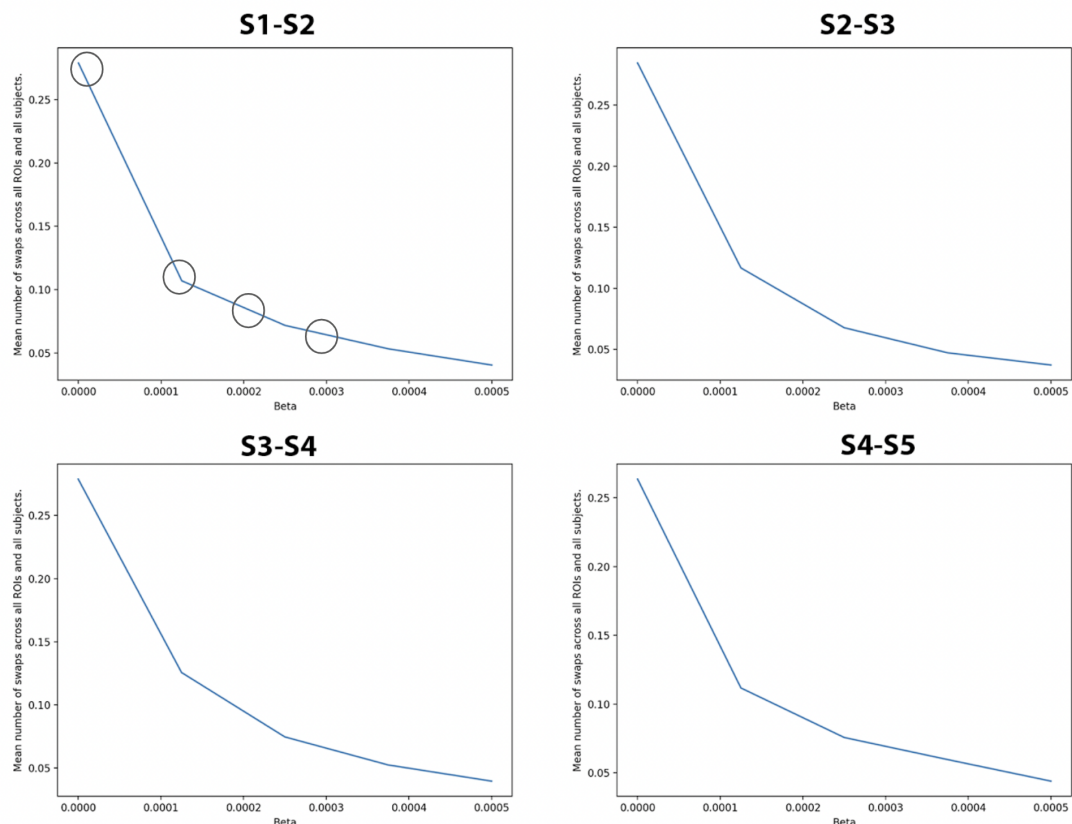


Figure S10: Proportion of swaps across all subjects and nodes with varying beta parameters. Circles in the top left figure indicate beta parameters chosen for subsequent analyses with varying β parameters.

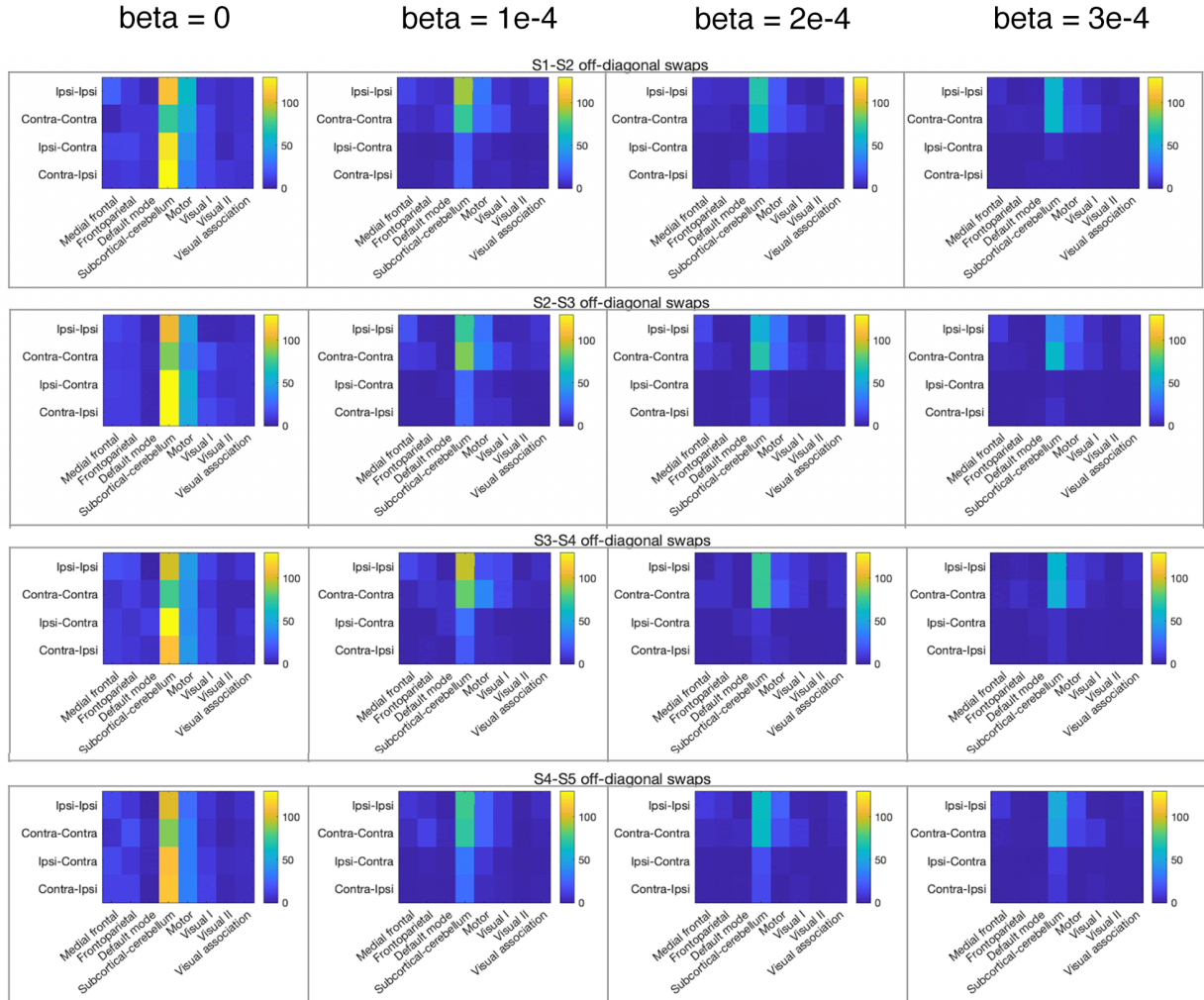
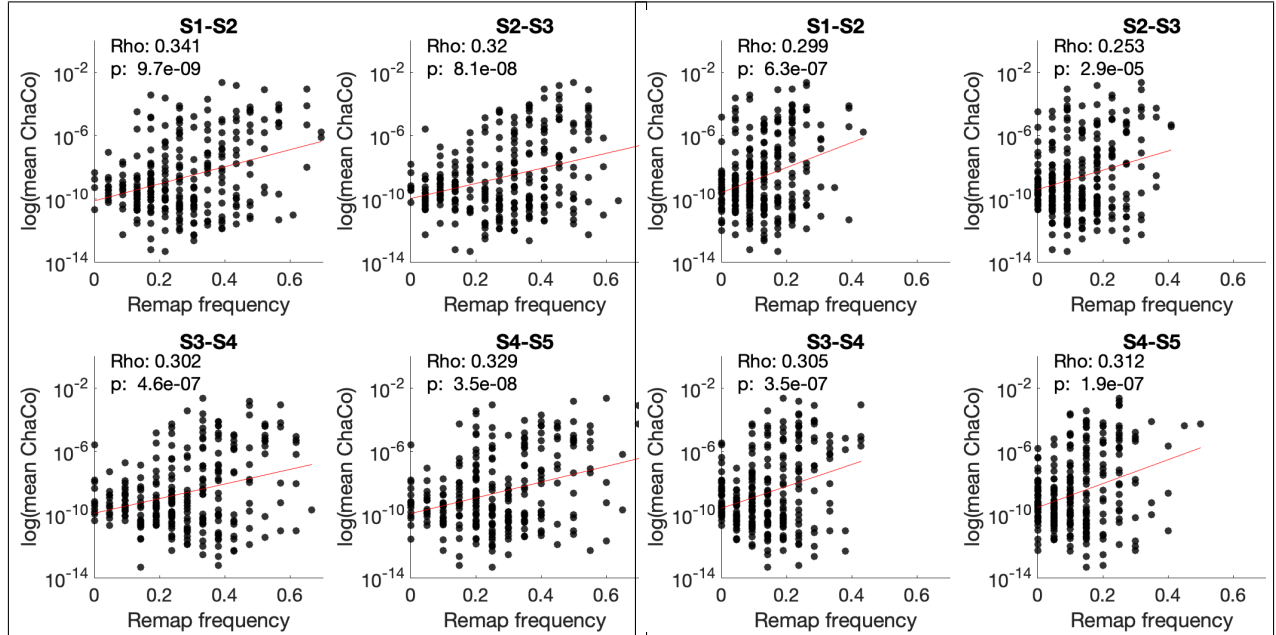
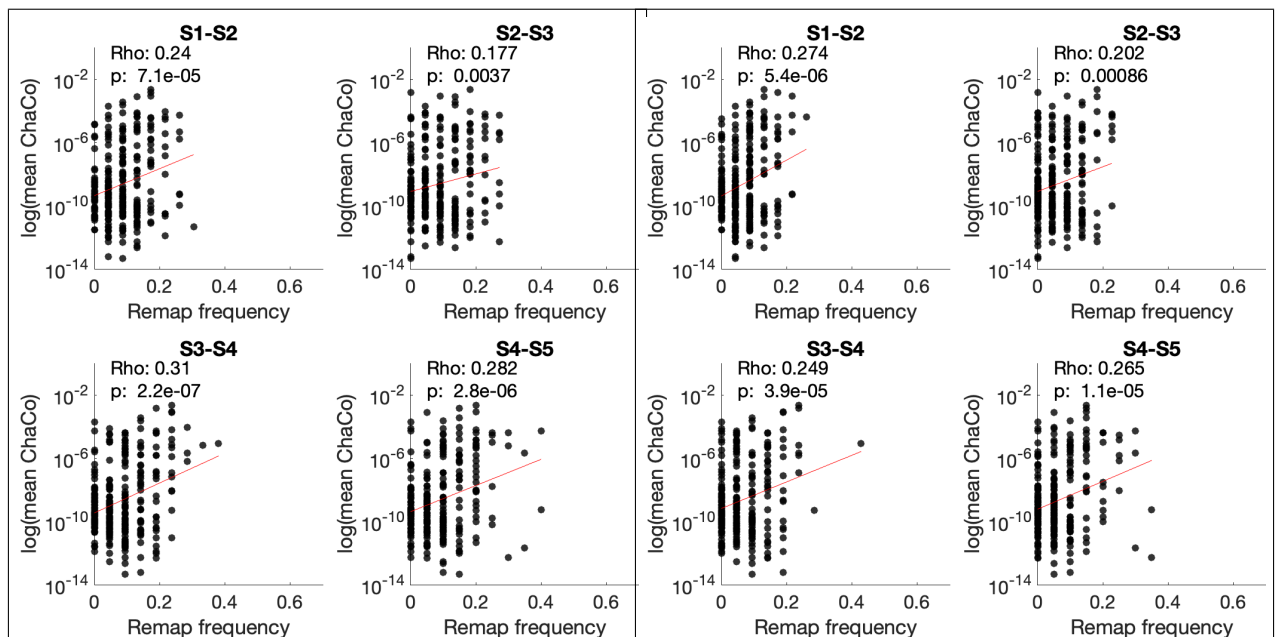


Figure S11: Impact of β on the sum of remaps within 8 functional networks, displayed separately depending on the source and target node's position relative to the lesion. (ipsilesional, same side as the lesion, and contralesional, opposite side as the lesion). Ipsi = ipsilesional, contra = contralesional. Ipsi-ipsi = ipsilesional node mapping to another ipsilesional node. Ipsi-contra = ipsilesional node mapping to a contralesional node. Contra-contra = contralesional node mapping to another contralesional node. Contra-ipsi = contralesional node mapping to an ipsilesional node.



(b) Beta 2 ($\beta = 1e-3$)



(d) Beta 4 ($\beta = 3e-3$)

Figure S12: Varying betas - correlation between number of remaps and ChaCo scores

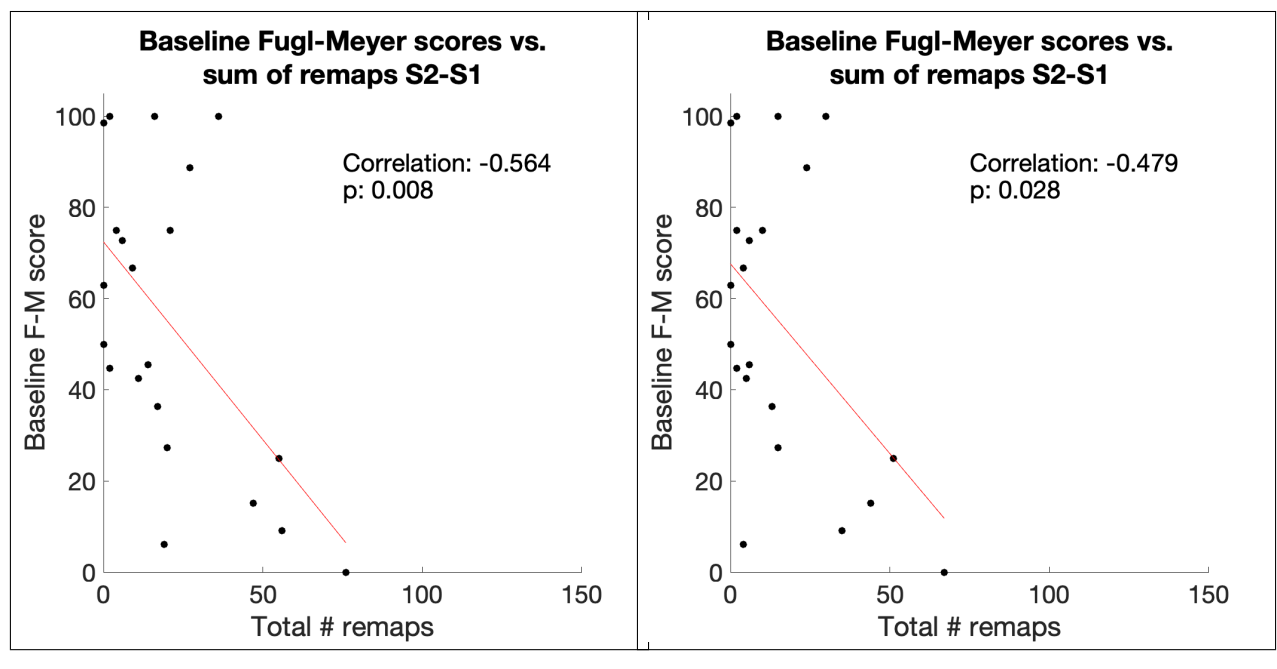
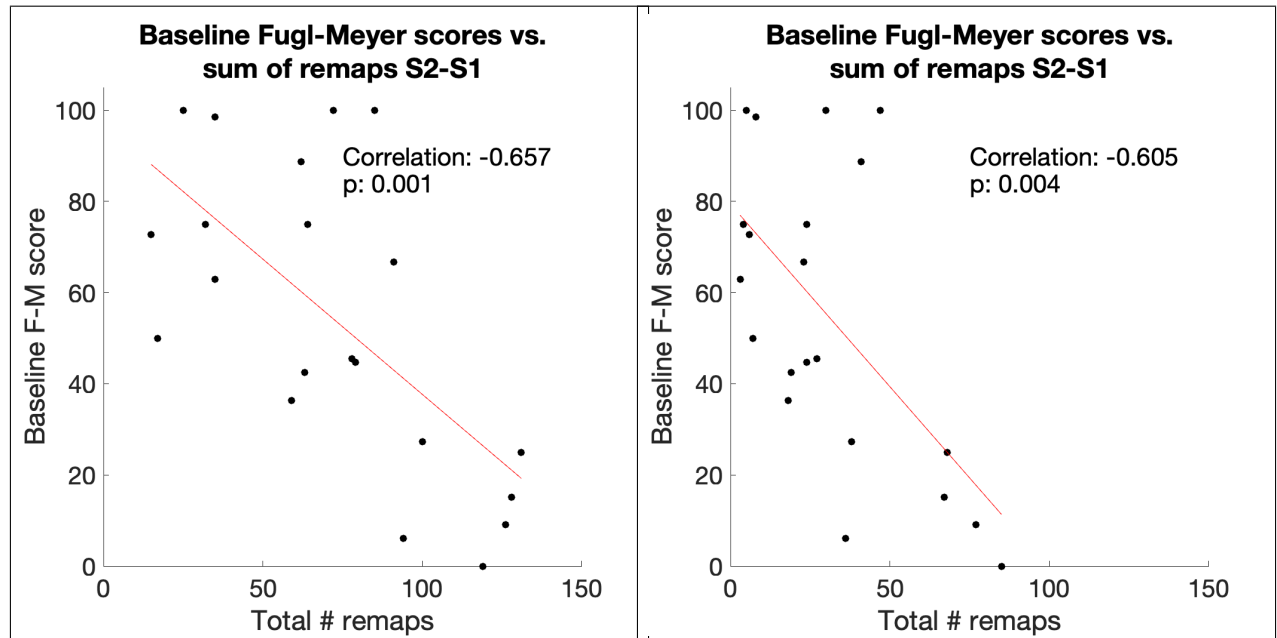


Figure S13: Varying beta does not change the significance of the relationship between total number of remaps between session 1 and session 2 and baseline Fugl-Meyer scores

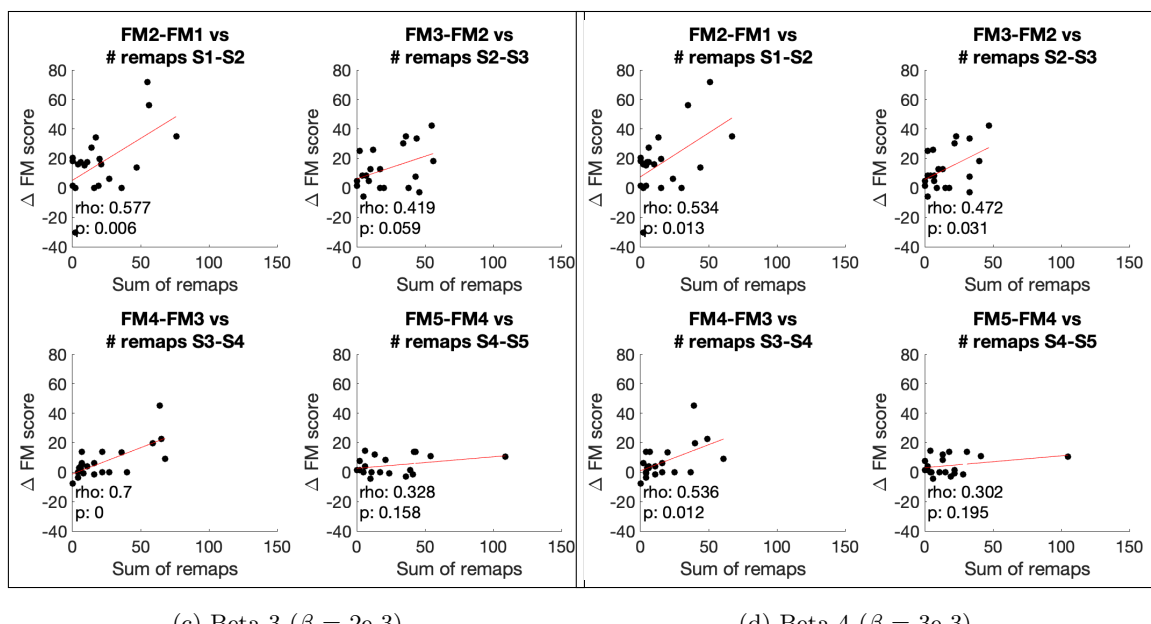
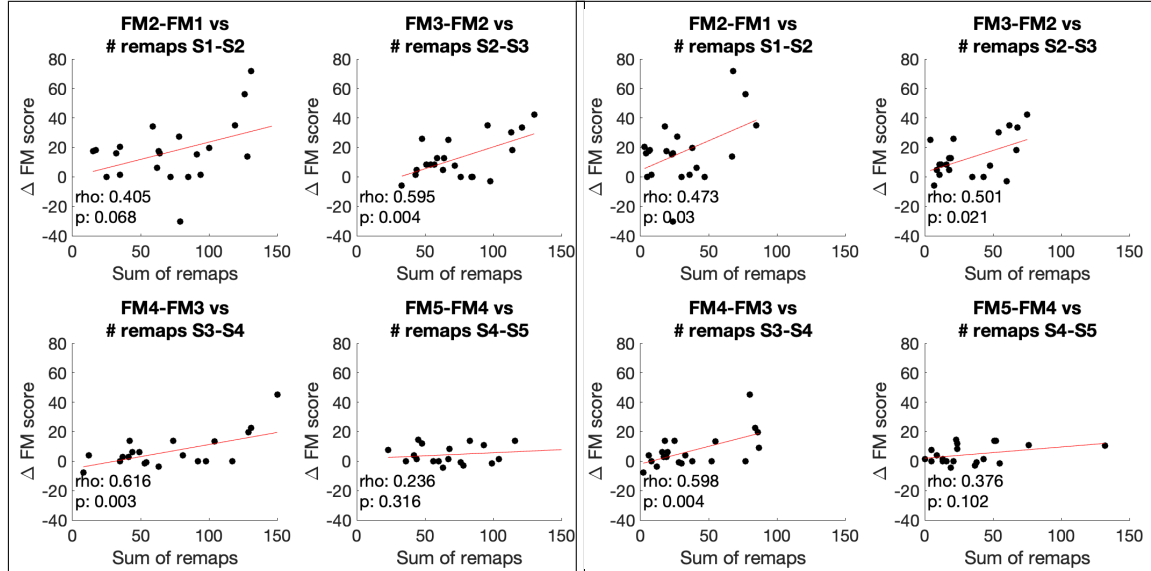


Figure S14: Varying beta generally does not alter the relationships observed between session-specific increases in Fugl-Meyer scores and the number of remaps between sessions.

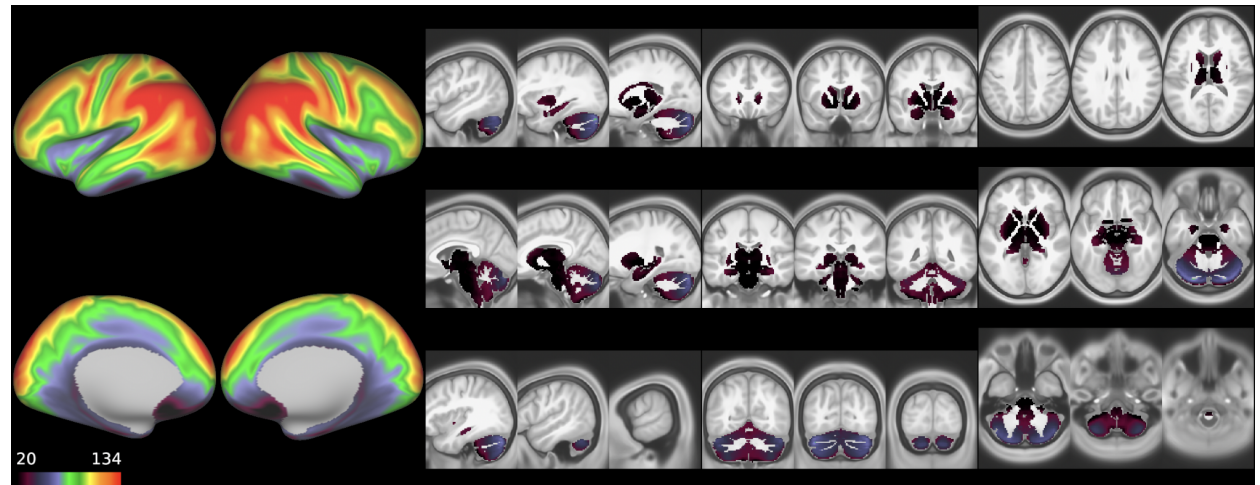


Figure S15: Keith's SNR calculations on the test-retest HCP data: temporal signal-to-noise ratio:
 $\text{TSNR} = \text{MEAN}/\text{stdev}(\text{non-artifact thermal noise})$

236 **References**

- 237 [1] P W Duncan, S M Lai, and J Keighley. “Defining post-stroke recovery: implications for design and
238 interpretation of drug trials”. en. In: *Neuropharmacology* 39.5 (Mar. 2000), pp. 835–841.
- 239 [2] Maurizio Corbetta et al. “Neural basis and recovery of spatial attention deficits in spatial neglect”.
240 en. In: *Nat. Neurosci.* 8.11 (Nov. 2005), pp. 1603–1610.
- 241 [3] Ian R Winship and Timothy H Murphy. “Remapping the somatosensory cortex after stroke: insight
242 from imaging the synapse to network”. en. In: *Neuroscientist* 15.5 (Oct. 2009), pp. 507–524.
- 243 [4] Ramina Adam et al. “Functional reorganization during the recovery of contralateral target selection
244 deficits after prefrontal cortex lesions in macaque monkeys”. en. In: *Neuroimage* 207 (Feb. 2020),
245 p. 116339.
- 246 [5] Yumi Murata et al. “Temporal plasticity involved in recovery from manual dexterity deficit after motor
247 cortex lesion in macaque monkeys”. en. In: *J. Neurosci.* 35.1 (Jan. 2015), pp. 84–95.
- 248 [6] Craig E Brown et al. “In vivo voltage-sensitive dye imaging in adult mice reveals that somatosensory
249 maps lost to stroke are replaced over weeks by new structural and functional circuits with prolonged
250 modes of activation within both the peri-infarct zone and distant sites”. en. In: *J. Neurosci.* 29.6 (Feb.
251 2009), pp. 1719–1734.
- 252 [7] Alex R Carter et al. “Resting interhemispheric functional magnetic resonance imaging connectivity
253 predicts performance after stroke”. en. In: *Ann. Neurol.* 67.3 (Mar. 2010), pp. 365–375.
- 254 [8] M A Urbin et al. “Resting-state functional connectivity and its association with multiple domains
255 of upper-extremity function in chronic stroke”. en. In: *Neurorehabil. Neural Repair* 28.8 (Oct. 2014),
256 pp. 761–769.
- 257 [9] Anne K Rehme and Christian Grefkes. “Cerebral network disorders after stroke: evidence from imaging-
258 based connectivity analyses of active and resting brain states in humans”. en. In: *J. Physiol.* 591.1
259 (Jan. 2013), pp. 17–31.
- 260 [10] Liang Wang et al. “Dynamic functional reorganization of the motor execution network after stroke”.
261 en. In: *Brain* 133.Pt 4 (Apr. 2010), pp. 1224–1238.
- 262 [11] Brenton Hordacre et al. “Fronto-parietal involvement in chronic stroke motor performance when cor-
263 ticospinal tract integrity is compromised”. en. In: *Neuroimage Clin* 29 (Jan. 2021), p. 102558.
- 264 [12] Eva-Maria Pool et al. “Network dynamics engaged in the modulation of motor behavior in stroke
265 patients”. en. In: *Hum. Brain Mapp.* 39.3 (Mar. 2018), pp. 1078–1092.
- 266 [13] Jie Lu et al. “Focal pontine lesions provide evidence that intrinsic functional connectivity reflects
267 polysynaptic anatomical pathways”. en. In: *J. Neurosci.* 31.42 (Oct. 2011), pp. 15065–15071.
- 268 [14] V Saia and L Pantoni. “Progressive stroke in pontine infarction”. en. In: *Acta Neurol. Scand.* 120.4
269 (Oct. 2009), pp. 213–215.
- 270 [15] Ying Wei et al. “Disrupted Regional Cerebral Blood Flow and Functional Connectivity in Pontine
271 Infarction: A Longitudinal MRI Study”. en. In: *Front. Aging Neurosci.* 12 (Nov. 2020), p. 577899.
- 272 [16] Caihong Wang et al. “Cerebral blood flow features in chronic subcortical stroke: Lesion location-
273 dependent study”. en. In: *Brain Res.* 1706 (Mar. 2019), pp. 177–183.
- 274 [17] G Liu et al. “Network change in the ipsilesional cerebellum is correlated with motor recovery following
275 unilateral pontine infarction”. en. In: *Eur. J. Neurol.* 26.10 (Oct. 2019), pp. 1266–1273.

- 276 [18] Emmanuel Carrera and Giulio Tononi. “Diaschisis: past, present, future”. en. In: *Brain* 137.Pt 9 (Sept.
277 2014), pp. 2408–2422.
- 278 [19] Donatello Conte et al. “Thirty Years Of Graph Matching In Pattern Recognition”. In: *Int. J. Pattern
279 Recognit Artif Intell.* 18.3 (May 2004), pp. 265–298.
- 280 [20] Yusuf Osmanlioğlu et al. “System-level matching of structural and functional connectomes in the
281 human brain”. en. In: *Neuroimage* 199 (Oct. 2019), pp. 93–104.
- 282 [21] X Shen et al. “Groupwise whole-brain parcellation from resting-state fMRI data for network node
283 identification”. en. In: *Neuroimage* 82 (Nov. 2013), pp. 403–415.
- 284 [22] Anirudh Wodeyar et al. “Damage to the structural connectome reflected in resting-state fMRI func-
285 tional connectivity”. In: *Network Neuroscience* (July 2020), pp. 1–22.
- 286 [23] Raphaël Liégeois et al. “Revisiting correlation-based functional connectivity and its relationship with
287 structural connectivity”. In: *Network Neuroscience* (Aug. 2020), pp. 1–17.
- 288 [24] A E Hillis et al. “Subcortical aphasia and neglect in acute stroke: the role of cortical hypoperfusion”.
289 en. In: *Brain* 125.Pt 5 (May 2002), pp. 1094–1104.
- 290 [25] Maurizio Corbetta et al. “Common behavioral clusters and subcortical anatomy in stroke”. en. In:
291 *Neuron* 85.5 (Mar. 2015), pp. 927–941.
- 292 [26] Amy Kuceyeski et al. “The Network Modification (NeMo) Tool: elucidating the effect of white matter
293 integrity changes on cortical and subcortical structural connectivity”. en. In: *Brain Connect.* 3.5 (2013),
294 pp. 451–463.
- 295 [27] Emily S Finn et al. “Functional connectome fingerprinting: identifying individuals using patterns of
296 brain connectivity”. en. In: *Nat. Neurosci.* 18.11 (Nov. 2015), pp. 1664–1671.